Stochastic Implementation of the Disparity Energy Model for Depth Perception

Kaushik Boga*, Naoya Onizawa‡, François Leduc-Primeau*, Kazumichi Matsumiya‡,
Takahiro Hanyu‡ and Warren J. Gross*
*Department of Electrical and Computer Engineering, McGill University, Montréal, Québec, Canada.
Email: kaushik.boga@mail.mcgill.ca, francois.leduc-primeau@mail.mcgill.ca, warren.gross@mcgill.ca
‡Tohuku University, Sendai, Japan.
Email: nonizawa@m.tohoku.ac.jp,kmat@riec.tohoku.ac.jp,hanyu@riec.tohoku.ac.jp

***Abstract*—We implement a binocular vision system based on a disparity-energy model that emulates the hierarchical multi-layered neural structure in the primary visual cortex. Layer 1 performs difference-of-Gaussian filtering that mimicks the center-surround receptive fields (RF) in the retina, layer 2 performs Gabor filtering mimicking the orientation selective filtering performed by simple cells and layer 3 has complex cells tuned to detecting 5 different disparities. A VLSI architecture is developed based on stochastic computing that is compact and adder-free. Even with a short stream length, the proposed architecture achieves better disparity detection than a floating-point version by using a modified disparity-energy model. A 1 $\times$ 100 pixel processing system is synthesized using TSMC 65nm CMOS technology and achieves up to 79% reduction in area-delay product compared to a fixed point implementation.**

I. Introduction

Measuring the relative depth of objects efficiently in real-time is a crucial issue as advances in robotics and artificial intelligence lead to ever smaller and more versatile devices with constrained resource budgets. Compared to conventional real-time image processing hardware implementations, biological vision achieves considerable power efficiency with high error resilience. Neuromorphic engineering aims to build hardware that exhibits these properties by taking inspiration from the structures and algorithms of biological systems. Ohzawa *et al.* proposed a disparity-energy model to express the disparity-selective properties of binocular complex cells in the primary visual cortex (V1) that are responsible for depth perception in the brain [1]. Binocular disparity measures the depth of objects using two images taken from different vantage points, and is defined as the difference in horizontal positioning of the same object in these two images [2]. This model has been shown to be valid in monkeys [3] and to describe well the response of binocular complex cells in V1 [4].

Several analog and mixed-signal VLSI vision chip implementations exhibiting low power and high area efficiency have been proposed [4]–[6]. These chips rely on analog transistor behavior to emulate the receptive field responses of neurons in V1. However, it is difficult to design highly-programmable analog circuits to describe higher-order neural behaviors compared to the digital counterparts [4]. They also do not scale easily to newer technology nodes and are sensitive to manufacturing variations. This motivates us to find digital implementations that exhibit similar characteristics to that of analog circuits. Stochastic computing (SC) bridges this gap by performing pseudo-analog operations in the digital domain.

This paper describes the VLSI implementation of a multi-layered neural network for the disparity-energy model using SC. We use *exponential compression* [7] to transform stochastic streams into the exponential domain where less precise stochastic additions are converted to precise stochastic multiplications, resulting in an adder-free architecture.

Section II first reviews SC and the disparity-energy model, then Section III presents a modification to the SC exponential compression technique [7]. Section IV presents the proposed system architecture. Implementation results are given in Section V and Section VI concludes the paper.

II. Background Material

A. Stochastic Computing

In SC, numbers are represented using random bit streams. We denote by P_x the probability that a bit in the stream is a 1. A *unipolar* SC encoding can represent a value $x \in [0,1]$ by choosing $P_x = x$ and a *bipolar* encoding can represent a value $x \in [-1,1]$ by choosing $P_x = (x+1)/2$. For example, a stream of 8 bits in unipolar encoding will represent $x = 0.5$ when 50% of the bit stream is composed of ones and 50% of zeros. SC allows for very simple circuit implementations of complex functions [8] [9]. For example, multiplication of two independent stochastic streams is performed with AND gate and scaled addition using a multiplexer. Since SC cannot represent numbers greater than 1, a multiplexer scales the output by 2 to represent the sum as a stochastic stream. Typically, numbers in conventional binary encoding are converted to stochastic streams by comparing the number with a sequence of uniformly-distributed random numbers, processed in the stochastic domain and converted back to binary numbers using counters that accumulate the bit stream [8]. Since SC uses unary bit streams where the position of a bit in the stream is inconsequential, it allows for graceful degradation in the presence of errors, in contrast to binary circuits [9].

In recent years, the field of SC has progressed rapidly and has demonstrated several practical implementations for applications ranging from LDPC decoders [10], [11], to image processing [9], [12] and neural network implementations [8]. These applications generally achieve good performance with relatively low-precision at corresponding stochastic stream lengths. However, a wider range of applications suffer from

978-1-4673-9604-2/15/.00

long latency due to high precision requirements. Even though multiplication in the stochastic domain is very efficient, addition is not. Due to the scaling involved in multiplexer based addition, for every two terms added, precision is reduced, leading to rapid precision loss when many numbers need to be added in the stochastic domain. This is usually compensated for by very long stream lengths, increasing latency and energy consumption. This paper addresses this by using the SC exponential compression technique presented in Section III, which allows an arbitrary number of terms to be added with less precision loss, significantly reducing the required length of the stochastic stream.

B. Disparity-energy model

When an object is perceived from left and right eyes, its position will be horizontally displaced in each of the corresponding images. The brain uses this horizontal disparity to estimate the relative depths of objects in three dimensions [1]. Zero disparity corresponds to those objects whose position is the same from both perspectives and excites corresponding retinal cells in each eye. Positive and negative disparities (corresponding to farther and closer objects) consequently will excite different retinal cells in each eye [4]. The disparity-energy model explains how the neural hierarchy in the brain processes this information to detect disparity. The model describes the hierarchy composed of binocular simple and complex cells. The image is first pre-processed by the retinal cells that have a concentric center-surround receptive field (RF), i.e. a positive center and negative surround (ON-center) or a negative center and positive surround (OFF-center) and fed into the disparity-energy model [4]. The pre-processing is best described by the Difference of Gaussian (DOG) filter [13], which approximates the 2D *Mexican hat wavelet* given by

$$\psi(x,y) = -\frac{1}{\pi\sigma^4}\left(1-\frac{x^2+y^2}{2\sigma^2}\right)e^{-\left(\frac{x^2+y^2}{2\sigma^2}\right)}. \quad (1)$$

The pre-processed images are fed to simple cells in both the left and right eye that have an orientation selective spatial RF, which can be approximated using 1D Gabor filters as

$$G_{\text{even}}(x) = \frac{1}{\sqrt{2\pi\sigma^2}}e^{-\frac{x^2}{2\sigma^2}}\cos\left(2\pi w_0 x\right), \quad (2)$$

$$G_{\text{odd}}(x) = \frac{1}{\sqrt{2\pi\sigma^2}}e^{-\frac{x^2}{2\sigma^2}}\sin(2\pi w_0 x). \quad (3)$$

These cells of the even (2) and odd (3) type have spatial receptive fields that differ by 90 degrees as shown in Fig. 1. In our implementation, we use the original disparity model introduced in [1], which uses simple cells that cannot fire negative responses. Hence, this model has four simple cells where each pair handles the positive and negative streams separately. Some other work such as [2], [4] used an equivalent model where the simple cell handles both positive and negative numbers, reducing the number of simple cells to two.

The even and odd Gabor responses from each eye converge onto binocular simple cells. The preferred disparity d for a particular cell is defined by the difference in the horizontal pixel positions that the even and odd Gabor responses are taken from. The complex cell C^d then takes the even and odd

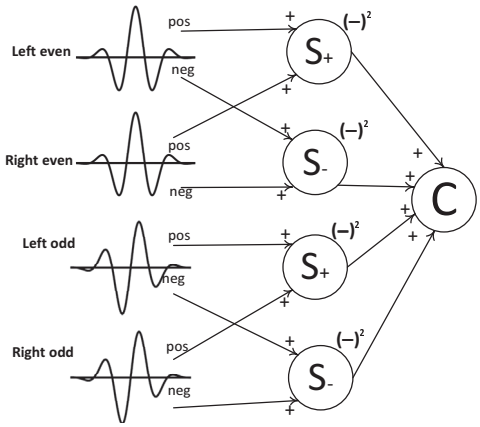

Fig. 1: Energy disparity model from [1] showing simple (S) and complex (C) cells.

binocular cell responses and squares and adds them [4]:

$$\begin{aligned} C^d(x_L,x_R) = &\left(G_{\text{even}+}\left(x_L+\frac{d}{2}\right)+G_{\text{even}+}\left(x_R-\frac{d}{2}\right)\right)^2 \\ &+\left(G_{\text{even}-}\left(x_L+\frac{d}{2}\right)+G_{\text{even}-}\left(x_R-\frac{d}{2}\right)\right)^2 \\ &+\left(G_{\text{odd}+}\left(x_L+\frac{d}{2}\right)+G_{\text{odd}+}\left(x_R-\frac{d}{2}\right)\right)^2 \\ &+\left(G_{\text{odd}-}\left(x_L+\frac{d}{2}\right)+G_{\text{odd}-}\left(x_R-\frac{d}{2}\right)\right)^2. \quad (4) \end{aligned}$$

In (4), x_L and x_R are the horizontal pixel positions for the left and right eye respectively, and $G_{even+}(x) = G_{even}(x)$ when $x > 0$ and 0 otherwise. The other Gabor functions are defined similarly. There are two ways of encoding disparity in the disparity-energy model: *position* shift and *phase* shift [2]. In this paper, we only use position shift, where d is defined by the difference in position of the receptive field.

III. Exponential Compression

The exponential compression method performs addition by transforming the stochastic streams of interest using an exponential function, such that additions are transformed into multiplications [7]. The exponential function is approximated by a Taylor series expansion of up to the third order. To implement the filters presented in Section IV, we must evaluate

$$z = \sum_i a_i x_i, \quad (5)$$

where a_i are the coefficients and x_i the system inputs. The corresponding stochastic circuit is shown in Figure 2. We assume that a_i and x_i have been properly scaled such that $|x_i| \leq 1$ and $|a_i| \leq 1$. The set $\{a_i\}$ of coefficients is partitioned into a set $\{a_i^+\}$ containing the positive coefficients, and a set $\{a_i^-\}$ containing the absolute values of the negative coefficients. Eq. (5) can be rewritten as

$$z = \sum_i a_i^+ x_i - \sum_i a_i^- x_i = \sum_i y_i^+ - \sum_i y_i^- = z^+ - z^-. \quad (6)$$

We also assume that $\sum a_i^- x_i \leq 1$ and $\sum a_i^+ x_i \leq 1$. We first perform the multiplications in (6) using AND gates to obtain

$y_i^+ = a_i^+ x_i$ and $y_i^- = a_i^- x_i$. To evaluate $\sum_i y_i^+$, we compress the individual streams $\{y_i^+\}$ as $\{e^{-y_i^+}\}$. The resulting set of compressed streams are multiplied together:

$$\prod e^{-y_i^+} = e^{-\sum y_i^+} = e^{-z^+}. \quad (7)$$

The $\{y_i^-\}$ streams are treated similarly. We obtain $z^+/2$ from e^{-z^+}, when we invert the exponential transformation by using a first order Taylor approximation of the natural logarithm:

$$z^+/2 \approx 1 - e^{-z^+}, \quad (8)$$

and similarly for $z^-/2$. Now, instead of accumulating for $z/2$ with an up-down counter fed by Z^+ and Z^- (where $\mathbb{E}[Z^+] = z^+/2$ and $\mathbb{E}[Z^-] = z^-/2$), to allow further stochastic processing, we transform the streams into Z_{pos} and Z_{neg}:

$$Z_{pos} = Z^+(1 - Z^-), Z_{neg} = Z^-(1 - Z^+) \quad (9)$$

When the streams Z^+ and Z^- are maximally correlated [14], $\mathbb{E}[Z_{\text{pos}}]$ and $\mathbb{E}[Z_{\text{neg}}]$ becomes

$$z_{\text{pos}} \approx \begin{cases} \frac{z^+ - z^-}{2} & \text{if } z^+ > z^-, \\ 0 & \text{otherwise} \end{cases} \quad z_{\text{neg}} \approx \begin{cases} \frac{z^- - z^+}{2} & \text{if } z^- > z^+, \\ 0 & \text{otherwise.} \end{cases} \quad (10)$$

Maximal correlation can be arranged by using a single noise source to generate all the x_i streams, and the same noise source for each pair of (a_i^+, a_i^-). z_{pos} and z_{neg} represent the positive and negative axis responses respectively of $z/2$; a property that allows re-use of stochastic streams for further processing.

The exponential compression block can be a Taylor order 1, 2 or 3 approximation and the circuits are presented in [7]. Note that our proposed implementation of exponential compression is different from [7] as we do not include an S-R latch at the output. The S-R latch leads to less precise addition, see Fig. 3b. The hold state of the S-R latch quickly saturates the stream towards 0 or 1 disallowing representation of intermediate numbers. As a result, we have reformulated the mathematical description from [7] as above to yield a better approximation.

Fig. 3a plots the Taylor expansions of order 1, 2, and 3 to the exponential function. Taylor order 1 is a poor approximation for large numbers, but is reasonably accurate for $|x| < 0.3$. As the expected value of the streams increases, higher order approximations should be used [7]. In this paper, a Taylor approximation of order 1 was sufficient to detect disparity. Also, note that a first order Taylor approximation is basically addition using OR gates. Fig. 3b shows the result of two-number addition with values ranging from -0.5 to 0.5 where each line shows the various Taylor approximations used, compared with exact addition.

IV. System Architecture

A three layer fully parallel 100x100 pixel processing circuit was implemented to detect 5 different disparity levels: $[-8, -4, 0, 4, 8]$. This architecture was inspired by [4] but we instead implement the system using stochastic computing. The stochastic processing architecture for a single pixel is shown in Fig. 4. The last stage of the circuit, shown inside the dashed box, contains binocular simple and complex cells tuned

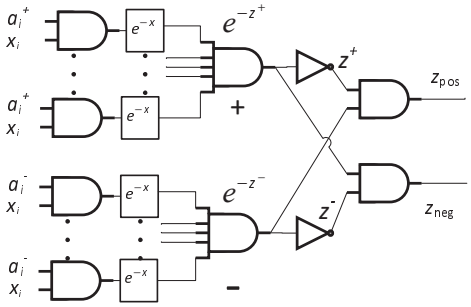

Fig. 2: Exponential convolution architecture.

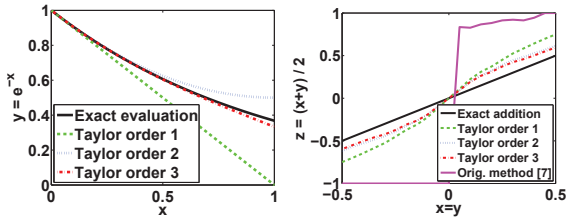

(a) Taylor approx. for e^{-x}. (b) Approx for $z = \frac{x+y}{2}$

Fig. 3: Taylor approximations

to detect one disparity. Overall, the single pixel processing stochastic circuit has 5 sets of binocular simple and complex cells (not shown) to detect the 5 disparity levels in parallel.

The concentric center-surround RF is implemented with a 2D DOG filter using a 5x5 kernel. The Orientation-Selective RFs are implemented with 1D Gabor filters using 1x9 Gabor kernels. The filtering stages are implemented using the stochastic exponential compression technique described in Section III. Each filtering stage takes a single stochastic stream as input and outputs a positive and a negative stream.

A. Gabor filters

The positive and negative stochastic streams from the stochastic DOG filters are processed separately using unipolar stochastic Gabor filters. After the second stage of filtering, each processed pixel is separated into four separate streams that we denote ++,- -, +- and -+. We combine ++ with - - into a first stream called even+, and +- with -+ into a second stream called even−. The even+ and the even− stream represent respectively the positive and negative axis response for the Gabor even filtered pixel. The odd+ and the odd− stream similarly represent the positive and negative axis response for the Gabor odd filtered pixel. These streams are then processed by simple and complex cells, described in Section IV-B.

1D Gabor even and odd filters convolved horizontally on an image respond maximally to vertical edges and show weakened response to increased angular orientation. The system was presented with bars oriented at angles varying from 0 to 180 degrees and the volume under the processed bar was measured for the Gabor even response and presented in Fig. 5 for stochastic implementations with stream lengths of 31 bits.The stochastic results are compared with a floating-point and a 6-bit fixed-point implementation. This is the minimum possible bit length where most of the filter coefficients can still be represented. All implementations can be seen to show similar

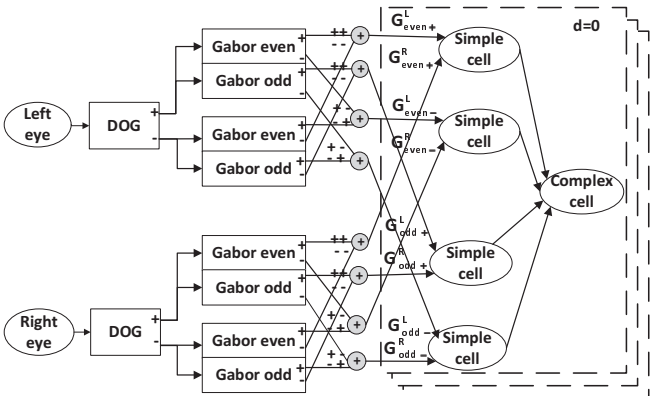

Fig. 4: System diagram for stochastic implementation.

orientation selectivity. The response of the stochastic system gets stricter as the order of the the exponential function's Taylor approximation is increased.

B. Complex cells

Whereas simple cells in (4) add filtered responses from each eye together before squaring them, the stochastic implementation presented here multiplies them before squaring:

$$C^d(x_L, x_R) = \left(G_{\text{even}+}\left(x_L + \frac{d}{2}\right) \cdot G_{\text{even}+}\left(x_R - \frac{d}{2}\right)\right)^2 + \left(G_{\text{even}-}\left(x_L + \frac{d}{2}\right) \cdot G_{\text{even}-}\left(x_R - \frac{d}{2}\right)\right)^2 + \left(G_{\text{odd}+}\left(x_L + \frac{d}{2}\right) \cdot G_{\text{odd}+}\left(x_R - \frac{d}{2}\right)\right)^2 + \left(G_{\text{odd}-}\left(x_L + \frac{d}{2}\right) \cdot G_{\text{odd}-}\left(x_R - \frac{d}{2}\right)\right)^2. \quad (11)$$

This modification allows for better disparity detection than the original model, see Fig. 6. The functionality of the binocular simple cell is to respond maximally when two converged streams have a positive response, and show an inhibitory response when those streams are mismatched, as modeled by the sum of squares in (4). We propose to replace the sum with a multiplication as in (11) because when there are mismatched responses, one of the streams will be 0 and multiplication by 0 eliminates this failed response. This acts as boolean checking of bit streams and helps to provide a positive response only for the disparity the simple and complex cells are tuned for.

To evaluate the effectiveness of disparity selectivity, the system was presented with impulse inputs. The responses measured from the complex cell tuned to d=0 are presented in Fig. 6. The impulse input response between the left and right eyes had a varying disparity difference from -12 to 12 pixels. Disparity selectivity using (11) is better for the stochastic implementation for bit stream lengths of 31 than the floating point and fixed point implementations using (4). Compared to the stochastic implementations, truncation and quantization noise highly weakens disparity selectivity for the fixed-point implementation. In post processing, though all implementations use a thresholding function to distinguish

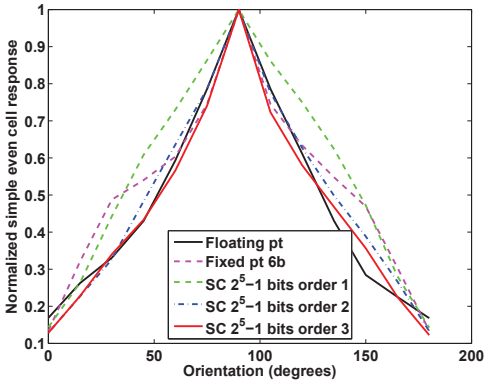

Fig. 5: Orientation selectivity curves for gabor even responses.

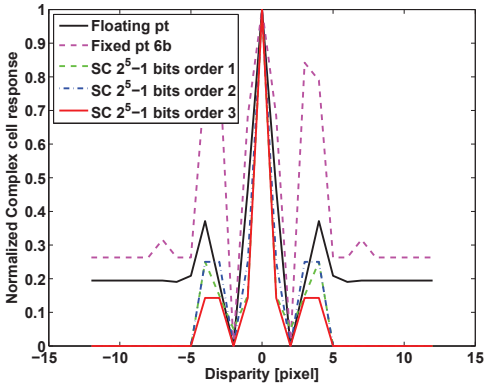

Fig. 6: Disparity selectivity curves for complex cell, d=0.

strong responses, the digital implementations require a variable threshold value to distinguish from the failed responses, which varies based on the stimuli. Due to the nature of ANDing in the stochastic implementation, a low fixed threshold value of 1 or 2 is usually sufficient to filter out the failed responses. Furthermore, we simplify the implementation of additions after Gabor filters and within the complex cells using OR gates because the stream densities are low enough for addition.

V. Results

For comparison, a conventional digital system using the original disparity-energy model given by (4) and a simple stochastic system using the modified model given by (11) were implemented. The conventional digital system uses 6-bit signed fixed-point number representation. The architecture is composed of 6-bit input multipliers and 9-bit input adders. The 12-bit multiplier output is truncated to 9 bits and these outputs are added together using 9-bit adders. This was the maximum truncation possible to minimize adder sizes before overflow and quantization significantly affected the results. We have chosen not to use the modified model for fixed point implementation because the multiplications in (11) would yield a larger circuit. The simple stochastic system uses bipolar number representation and additions in the filtering stages are implemented with multiplexers. Note that a 6-bit signed fixed point or 6-bit bipolar stochastic implementation correspond to a 5-bit unipolar stochastic implementation. When signed number representation is used, the model in Fig. 1 is simplified to use two simple cells only [2]. Filtered images are not shown

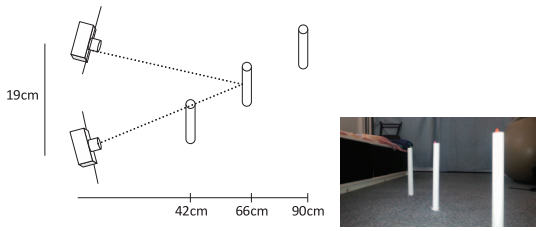

(a) Experimental setup. (b) Right view.

Fig. 7: Experiment to detect disparity.

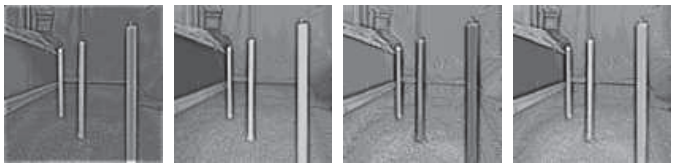

(a) Fix-pt 6b. (b) SC order 1. (c) SC order 2. (d) SC order 3.

Fig. 8: DOG filtered outputs with SC length = 2^5-1.

for the simple stochastic implementation because the filters are non-functional at equivalent bit stream lengths.

A. Experiment setup

To detect the depth of objects, an experiment was setup similar to [4] as shown in Fig. 7(a). The cameras were setup 19 cm apart with an 8 degree angle from the vertical. As a result, the fixation point (the point at the intersection of the line of sight of each camera) is 66 cm away. At this range, disparity corresponds to around 3 cm per pixel. We place one white pole on the fixation point. To detect disparities of -8 and +8, two white poles were placed at a distance of 42 and 90 cm respectively from the cameras center. These poles sit on a circle with a 60 cm diameter.

B. Filter outputs

Figures 8, 9 and 10 present DOG, Gabor even and Gabor odd filtered responses from the right eye image for different implementations. The images have been normalized, and the streams accumulated using counters for presentation. The difference in brightness for some images is a result of normalization. Visually, all implementations are similar to the fixed point implementation. The slight differences between the $2^5 - 1$ bit proposed stochastic implementations compared to the fixed point implementation can be resolved as the length of the stochastic stream is increased. Despite this, due to the highly robust nature of the algorithm, disparity is still strongly detected, see Fig. 12.

C. Disparity detection

Figures 11, 12 and 13 present the disparity maps for the floating point, proposed stochastic and simple stochastic implementations respectively. Figures 11 (f), 12 (f) and 13 (f) postprocessed in MATLAB use [blue, cyan, green, yellow, red] when disparities of [+8,+4,0,-4,-8] are detected. The proposed stochastic implementation uses an exponential Taylor order 1

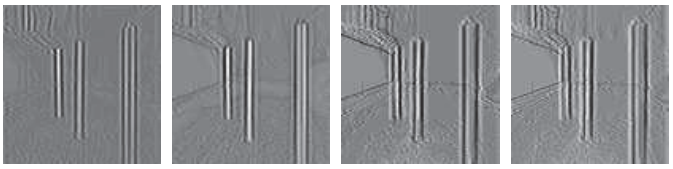

(a) Fix-pt 6b. (b) SC order 1. (c) SC order 2. (d) SC order 3.

Fig. 9: Gabor even filtered outputs with SC length = 2^5-1.

(a) Fix-pt 6b. (b) SC order 1. (c) SC order 2. (d) SC order 3.

Fig. 10: Gabor odd filtered outputs with SC length = 2^5-1.

approximation with a bit stream length of 31 bits. Figures 11 and 12 detect the relative positions of the three poles correctly.

As can be seen from Fig. 13, at stream lengths of $2^6 - 1$, the simple stochastic system is non-functional. No value for thresholding manages to distinguish the objects correctly. For the simple stochastic implementation to achieve similar performance, we need bit stream lengths in excess of 2^{16} due to the low precision nature of multiplexer based addition. The proposed implementation achieves the same with $2^5 - 1$ bits.

VI. Synthesis results

To synthesize the circuit, we first synthesize a component implementing the processing for 1x100 pixels. This component is then simply instantiated 100 times in order to obtain a full 100x100 system. The 1x100 pixel processing system was synthesized using Cadence RC compiler for TSMC 65 nm CMOS technology and area results are presented in Table 1. Stochastic circuit area results are presented for Taylor approximations of 1st, 2nd and 3rd orders. For comparison, a 6b signed fixed point implementation was chosen. When interface circuitry (linear feedback shift registers (LFSRs) for random number generation, comparators and counters) to convert from digital to stochastic domain and back are included, total area of the stochastic circuit expands to 0.28 mm^2, 0.51 mm^2 and 0.69 mm^2 for Taylor orders 1, 2, and 3 respectively. This leads to a stochastic area increase of 150%, 49% and 31% for each of the stochastic Taylor approximations. Even if interface circuitry is included, stochastic circuits yield very low area compared to the fixed point implementation for all Taylor approximations. It should be noted that if further visual processing is to be done in the stochastic domain, the overhead is only incurred once, at the input and output of the entire SC system. Note that the input and output ports to the circuits presented in Table 1 are registered.

The stochastic implementation has a latency of L clock cycles where L represents the stochastic stream length used to represent the numbers. The fixed point equivalent runs in a single clock cycle but needs a very large area. For allowing a comparison, we use the area $\times$ delay product (ADP) measure.

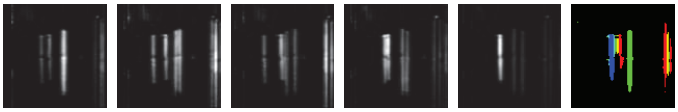

(a) d=0. (b) d=-4. (c) d=-8. (d) d=4. (e) d=8. (f) all-inc.

Fig. 11: Disparity maps (floating-point).

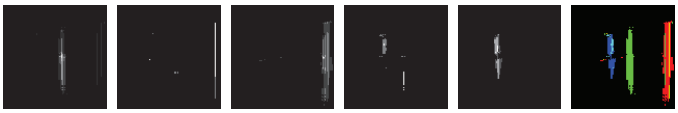

(a) d=0. (b) d=-4. (c) d=-8. (d) d=4. (e) d=8. (f) all-inc.

Fig. 12: Disparity maps (Proposed SC 2^5-1 bits Taylor ord. 1).

As presented in Table 2, the ratio of stochastic to digital ADP estimates are lower or equivalent for all three approximations. If interface circuitry is used in this calculation, the stochastic to fixed point ratio increases to 0.54, 0.96 and 1.32 respectively for each of the three Taylor approximations. The circuit can be pipelined further to increase throughput since it is a purely feed forward architecture, but the latency will remain unchanged.

VII. Discussion and Conclusion

In this paper, we presented a stochastic VLSI architecture and implementation of the disparity-energy model for depth perception. The modified stochastic disparity-energy model is more effective at inhibiting failed responses than the floating point version for the original model and enables disparity detection at very low stream lengths of $2^5 - 1$ bits. This low stream length was achieved as a result of our adder-free architecture which leads to minimum scaling loss, allowing us to implement a multi-stage stochastic architecture without the need for long processing times.

For this application, a first order Taylor approximation was sufficient to detect disparity because stream densities are low. However, as increasing accuracy in computations is desired, increasing Taylor order approximations for the exponential function should be used. The synthesis results suggest that stochastic implementations of the disparity-energy model are

TABLE I: Synthesis results.

Instance (1x100)	Logic cell count	Total Area $[mm^2]$	Clock period $[ns]$	Area ratio
SC order 1	16.2k	0.11	1.7	0.02
SC order 2	58.4k	0.34	1.7	0.06
SC order 3	77.9k	0.53	1.7	0.09
Fixed pt 6b	781k	5.64	4.9	1

TABLE II: Area-Delay Product (ADP).

Instance (1x100)	Delay (ns)	ADP $[mm^2 \cdot ns]$	ADP ratio
SC order 1	1.7 x 31	5.9	0.21
SC order 2	1.7 x 31	17.9	0.65
SC order 3	1.7 x 31	27.9	1.01
Fixed pt 6b	4.9 x 1	27.6	1

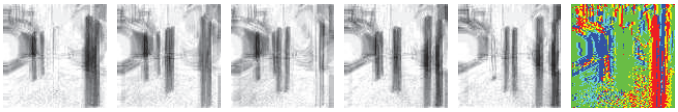

(a) d=0. (b) d=-4. (c) d=-8. (d) d=4. (e) d=8. (f) all-inc.

Fig. 13: Disparity maps (Simple SC bipolar $2^6 - 1$ bits).

very area-efficient and show a low ADP compared to the digital counterpart. We believe that stochastic computing has the potential for efficient digital implementations of large scale neuromorphic models. Future work will implement real-time stochastic Gabor filters [15] to generate Gabor filter coefficients in the stochastic domain without needing to pre-compute them digitally and convert them to stochastic streams.

Acknowledgments

The authors would like to thank Arash Ardakani and Xinchi Chen for useful discussions. Warren J. Gross is a member of ReSMiQ and SYTACom. This work was supported by the Brainware LSI Project of MEXT, Japan.

References

[1] I. Ohzawa, G. C. Deangelis, and R. D. Freeman, "Stereoscopic depth discrimination in the visual cortex: neurons ideally suited as disparity detectors," *Science*, vol. 249, no. 4972, pp. 1037–1041, 1990.

[2] N. Qian, "Binocular disparity and the perception of depth," *Neuron*, vol. 18, no. 3, pp. 359–368, 1997.

[3] B. Cumming and A. Parker, "Responses of primary visual cortical neurons to binocular disparity without depth perception," *Nature*, vol. 389, no. 6648, pp. 280–283, 1997.

[4] K. Shimonomura, T. Kushima, and T. Yagi, "Binocular robot vision emulating disparity computation in the primary visual cortex," *Neural Networks*, vol. 21, no. 2, pp. 331–340, 2008.

[5] T. Y. W. Choi, P. A. Merolla, J. V. Arthur, K. A. Boahen, and B. E. Shi, "Neuromorphic implementation of orientation hypercolumns," *IEEE Trans. Circuits Syst. I, Reg. Papers*, vol. 52, no. 6, 2005.

[6] S.-C. Liu, J. Kramer, G. Indiveri, T. DelbruÈck, T. Burg, and R. Douglas, "Orientation-selective aVLSI spiking neurons," *Neural Networks*, vol. 14, no. 6, pp. 629–643, 2001.

[7] C. Janer, J. Quero, J. G. Ortega, and L. G. Franquelo, "Fully parallel stochastic computation architecture," *IEEE Trans. Signal Process*, vol. 44, no. 8, pp. 2110–2117, 1996.

[8] B. D. Brown and H. C. Card, "Stochastic neural computation. i. computational elements," *IEEE Trans. Comput.*, vol. 50, no. 9, 2001.

[9] P. Li, D. J. Lilja, W. Qian, K. Bazargan, and M. D. Riedel, "Computation on stochastic bit streams digital image processing case studies," *IEEE Trans. Very Large Scale Integr. (VLSI) Syst*, vol. 22, no. 3, 2014.

[10] F. Leduc-Primeau, V. C. Gaudet, and W. J. Gross, "Stochastic decoders for LDPC codes," in *Advanced Hardware Design for Error Correcting Codes*. Springer, 2015, pp. 105–128.

[11] S. S. Tehrani, A. Naderi, G.-A. Kamendje, S. Hemati, S. Mannor, and W. J. Gross, "Majority-based tracking forecast memories for stochastic LDPC decoding," *IEEE Trans. Signal Process*, vol. 58, no. 9, 2010.

[12] A. Alaghi, C. Li, and J. P. Hayes, "Stochastic circuits for real-time image-processing applications," in *Design Automation Conference*, 2013.

[13] M. J. McMahon, O. S. Packer, and D. M. Dacey, "The classical receptive field surround of primate parasol ganglion cells is mediated primarily by a non-gabaergic pathway," *The Journal of neuroscience*, vol. 24, no. 15, pp. 3736–3745, 2004.

[14] A. Alaghi and J. P. Hayes, "Exploiting correlation in stochastic circuit design," in *Computer Design (ICCD), 2013 IEEE 31st International Conference on*. IEEE, 2013, pp. 39–46.

[15] N. Onizawa, D. Katagiri, K. Matsumiya, W. Gross, and T. Hanyu, "Gabor filter based on stochastic computation," *IEEE Signal Process. Lett.*, vol. 22, no. 9, pp. 1224–1228, Sept 2015.